Aninat, R., Zoppi, G., Forbes, I. and Miles, R.W. (2010) ' Formation of Cu(In1-xAlx)Se2 by selenising RF magnetron sputtered Cu/Al/In precursor layers'. Proceedings of the 6th Photovoltaic Science Applications and Technology (PVSAT-6), University of Southampton, 24-26 March, The Solar Energy Society, pp. 185-188.

Formation of $Cu(In_{1-x}Al_x)Se_2$ by Selenising RF Magnetron Sputtered Cu/Al/In Precursor Layers

R.Aninat[a*], G.Zoppi[a], I.Forbes[a], R.Miles[a]

[a] *Northumbria Photovoltaics Applications Centre, Northumbria University, Ellison Building, NE1 8ST, UK*

**corresponding author. E-mail: r.aninat@northumbria.ac.uk*

Introduction

$Cu(In_{1-x}Al_x)Se_2$ (CIAS) is an alloy of $CuInSe_2$ (CIS, energy bandgap, 1.0eV) and $CuAlSe_2$ (CAS, energy bandgap, 2.7eV). In principle it should be possible to alter the energy bandgap of the CIAS from 1.0eV to 2.7eV by altering the alloy composition, x, if there is complete miscibility of the constituent compounds across the full composition range. In particular, it is possible that high efficiency cells could be produced with energy bandgaps >1.5eV, the optimal bandgap for single junction cells [i], and making it possible to fabricate tandem devices using CIAS upper cells and CIS lower cells. This is not possible with CIGS ($Cu(In_{1-x}Ga_x)Se_2$) based devices as increasing the Ga content in CIGS to produce energy bandgaps >1.16eV results in a rapid drop in device efficiency, this being attributed to the high Ga content degrading the material quality of the CIGS [ii] [1]. A comparable aluminium content in CIAS corresponds to an energy bandgap of 1.38 eV. This is wider than for CIGS because the energy bandgap of CAS is much wider than that of CGS($CuGaSe_2$).

In this work, the CIAS films have been prepared using a two-stage process, the deposition of Cu/Al/In precursor layers by r.f. magnetron sputtering followed by annealing the precursors in a selenium containing environment using temperatures in the range 450-550ºC and for times in the range 10-30 minutes. The $Cu(In_{1-x}Al_x)$ precursors were deposited with four different layouts and 3 different Al contents, and finally coated with a thin film of selenium and annealed in a Se environment to convert them into the compound. The simplest layout was a simple alloy of Cu, In and Al, whereas the more complicated ones were designed to overcome the diffusion of Al and In which resulted in a separation of CAS and CIS phases.

This work reports on the chemical and physical properties of the layers formed when investigated using scanning electron microscopy to observe the surface topology and topography, energy and wavelength dispersive x-ray analysis to determine the film composition, x-ray diffraction to determine the phases present and structure of each phase and secondary ion mass spectroscopy to determine the compositional profile of each element present in the samples.

Experimental

Precursor deposition

Soda Lime Glass (SLG) was used as a substrate. The precursor material was deposited by radio frequency (RF) sputtering in a *Nordiko 2000*, using three elemental targets of Cu, In and Al. The substrate table was rotated below the targets at a speed of 10 rounds per minute, in order to get a superposition of thin layers (a few nanometres thick) of each element. Set A was deposited with a medium Al content by applying a typical set of power to the targets. Set B was sputtered with a higher Al content, and covered with a thin (≈10nm) Cu cap. Finally, sets Y and Z were deposited with a different design, consisting of a superposition of a CuIn layer and a CuInAl, to overcome the migration of Al and In. Additionally, set Z was covered with a 100nm Cu cap (set Z), to prevent the oxidation of the surface.

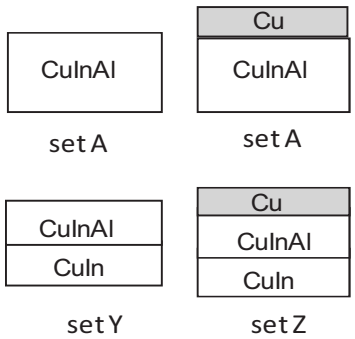

Figure 1: layout of the precursors

Film conversion

For each set, different thicknesses of selenium were then evaporated on top of the precursors in a *Nano 38* evaporator, and the samples were subsequently annealed in either a Large Tube Furnace (LTF) or a Rapid Thermal Processor (RTP). The main difference between these two types of furnaces relies in the physical heating process. The LTF utilises heating coils located around the chamber, whereas RTP makes use of lamps that heat the sample. The main advantage of the LTF is its size, which allows one to anneal several samples at a time (up to 6), and provides a very uniform heating across the chamber. However, this mode of heating results in a very long cooling time (more than 10hours). The RTP chamber is designed to anneal no more than 3 samples at once, but only requires an hour to cool down. Besides, it allows a very good control over all the annealing parameters, especially the ramping rate, and multiple step processes can be set. The RTP furnace was used preferentially for this work. The base pressure in both furnaces was typically of 3.10^{-3} mbars, and H2/N2 was fed into the chamber prior to the reaction in order to enhance the conversion of the precursor. A 10mbars starting pressure is used in the LTF process, whereas 100mbars was found more suitable for the RTP process.

Characterisation

The composition of the precursors was systematically measured by Energy Dispersive Spectroscopy (EDS) prior to Se coating and subsequently to annealing. Scanning Electron Microscope (SEM) images were used in complement to EDS and Wavelength Dispersive Spectroscopy (WDS) to study the cross section. The crystallographic phases in the precursor and the annealed materials were characterised by X-ray diffraction (XRD), and the composition once more analysed by EDS. When relevant, Secondary Ion Mass Spectroscopy (SIMS) was used to determine the compositional depth profile of the films. Finally spectrophotometry was undertaken to assess the bandgap(s) of the film.

Results and discussion

Precursors

After deposition, the composition of the precursors was measured by EDS. The typical results are indicated in Table 1.

Set	Cu	In	Al	x
A	49	31.5	19.4	0.38
B*	54.99	24.86	20.15	0.45
Y*	46.1	38.7	15.2	0.28
Z*,**	59.2	34.9	5.9	0.15

Table 1: EDS composition of the precursors

* *Note the burying of the CuIn layer affects the EDS measurements*
** *The Cu cap affects the measurements*

Regarding the uniformity of the precursors, glow discharge measurements show relatively uniform distribution of the three elements (Figure 2).

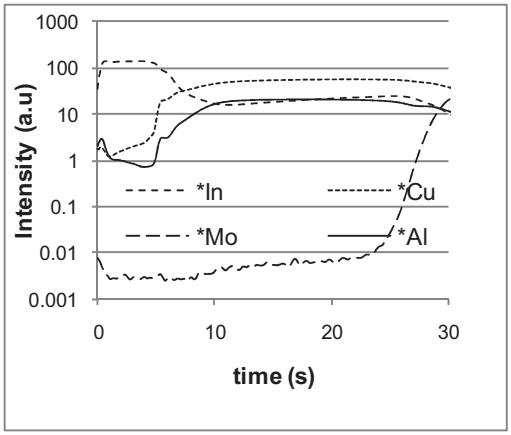

Figure 2: Glow discharge depth profile of a precursor from set A

RTP conversion

The films were converted under various conditions of temperature and dwelling time. The main indicator used to detect the presence of CIAS was the shifting of the (112) peak of the CIS (Figure 3).

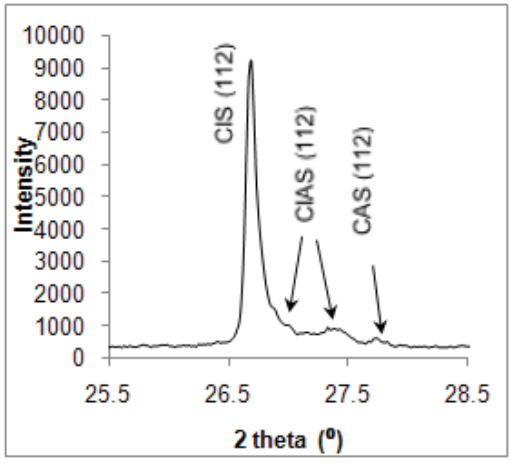

Figure 3: XRD of a sample set A annealed with process d, presenting CIS, CIAS and CAS phases

The results of conversion are summarised in Table 2.

sample set	CIS	CIAS shift	CAS	process
A	yes	26.86	**no**	***a***
Y	yes	26.86*	yes	***a***
Z	yes	none	yes	***a***
Y	yes	26.84	yes	***b***
Z	yes	26.9	yes	***b***
A	yes	26.8*	yes	***c***
A	yes	27.18	yes	***d***
A	yes	none	yes	***e***
A	yes	none	yes	***f***
A	yes	none	yes	***g***

Table 2: annealing results obtained in the Rapid Thermal Processor

* *Very little peak*

process	ramp time	dwell time	temp.
a	130s	610s	350ºC
b	130s	1800s	360ºC
c	550s	1800s	420ºC
d	600s	1800s	450ºC
e	1150s	1800s	450ºC
f	800s	1200s	480ºC
g	800s	1200s	500ºC

Table 3: annealing process summary

From the data summarised in Table 2, we can extract several pieces of information:

First, all the samples annealed below 390^{0}C consistently grew CIAS and CIS, with the exception of sets Y and Z. We also notice that in the case of set A, CAS tends to form less at lower temperature. As the temperature is increased to 450^{0}C, the reproducibility becomes very poor, and no CIAS could be grown beyond this temperature in the RTP. Finally, a notable phenomenon is the growth of CIS in all the films.

Cross section and EDS/WDS analyses

The cross section of the samples that grew both CIS and CIAS, like set *e*, shows that two layers formed (Figure 4). The WDS and EDS measurements performed on the cross section show that layer 1 is Al rich and In poor, whereas layer 2 is In rich and Al poor (Figure 5). That means that Al has migrated towards the back contact and In has migrated towards the top of the film. Layer 1 (≈700nm) is characteristic by his small grain size, and is most likely CAS at the bottom and CIAS at the interface with layer 2. Layer 2 (≈1.5µm) on the other hand displays much bigger grains, and seems to correspond to the CIS phase in the XRD spectrum.

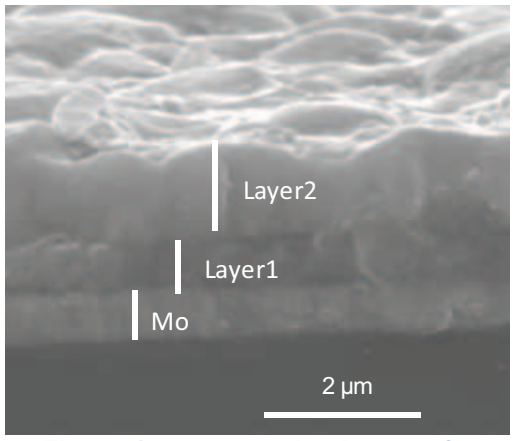

Figure 4: cross section image of a sample showing both CIS and CIAS phases

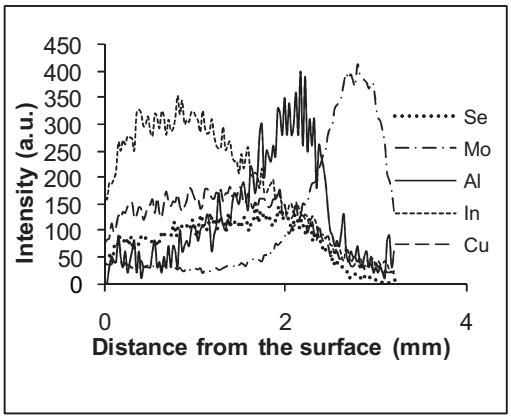

Figure 5: WDS/EDS analyses of the cross section of a sample showing CIS and CIAS phases

Using these results, we can interpret the bad conversion of sets Y and Z annealed via the process a: as mentioned before, sample sets Y and Z were designed to deal with the tendency of Al and In to migrate. However, the Al is all contained within the top layer, and hence requires more time to diffuse through the sample. In process a, the dwelling at temperature is too short (≈600s) and only CAS is formed. In process b, on the other hand, the longer dwelling time (1800s) gives time for the Al to diffuse and the CIAS to form. A last interesting point is the differences observed between sets Y and Z. Whereas samples from set Y displayed poor adhesion and poor cristallinity, Z shows sharper and bigger CIAS peaks. This indicates that oxidation happens in set Y which is prevented by the Cu cap topping the samples from set Z. However, further analysis would be required to determine the exact effects of oxidation.

LTF conversion

The results obtained with the LTF are summarised in Table 4.

sample set	A	A	B
x	0.38	0.15	0.44
CIS?	yes	yes	**no**
CIAS shift	27.02	27.34	26.86
CAS?	yes	yes	**no**
extra peaks	no	no	27.22 27.88
process	*h*	i	h
Reproducibility	good		good

Table 4: annealing results obtained with the Large Tube Furnace

Set A grew CIAS but the adhesion was generally poor. XRD spectra of set B on the other hand show CIAS phases alone were consistently grown, even though the cristallinity was quite poor.

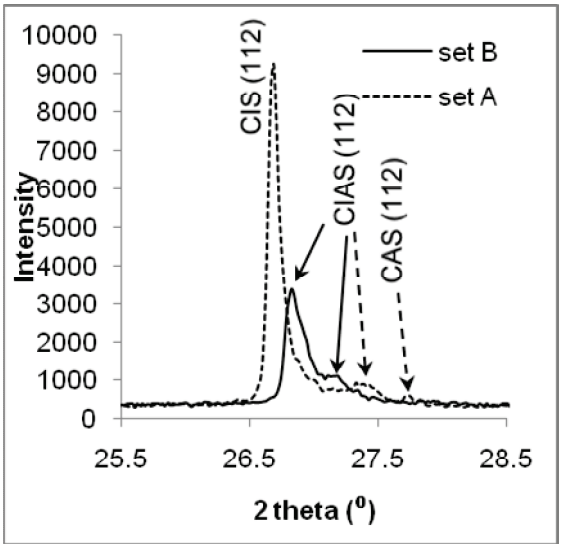

Figure 6: comparison of XRD spectra of sets A and B

[i] J. J. Lofersky et al., *Journal of Applied Physics* vol. 27, p. 777, 1956.

[ii] I. Repins, M. A. Contreras et al., *Progress in Photovoltaics,* vol. 16, pp. 235-239, May 2008.